CrossMark

ORIGINAL PAPER

Grafting of thermosensitive poly(*N*-isopropylacrylamide) from wet bacterial cellulose sheets to improve its swelling-drying ability

Rasim Alosmanov · Karol Wolski · Szczepan Zapotoczny

Abstract Thermoresponsive poly(*N*-isopropylacry-lamide) (PNIPAM) is grafted from wet bacterial cellulose (WBC) sheets using atom transfer radical polymerization (ATRP). WBC is recognized as a highly swollen biocompatible material with broad application potential. However, native WBC undergoes drying relatively fast and its reswelling ability diminishes after losing a substantial amount of water. In this work PNIPAM is grafted from WBC to slow down its drying, especially at elevated temperatures, which is relevant for biomedical applications. As a primary step, initiator molecules, 2-bromoisobutyryl bromide, are attached to WBC through linkers that are covalently bound to the cellulose hydroxyl groups. Grafting of PNIPAM is then realized via surface-initiated ATRP in a water/methanol mixture leading to WBC-g-PNIPAM. The modification steps are followed via FT-IR, XRD, elemental analysis, and atomic force microscopy. It is concluded that PNIPAM contributes to ca. 22% of the dry mass of WBC-g-PNIPAM. The samples are subjected to repeating swelling and drying steps at 25 °C and drying at 40 °C. The obtained results indicate that grafted PNIPAM significantly reduces drying of the modified WBC and enables better reswelling after treatment at 40 °C with respect to native WBC. The reported synthetic method may also be used for grafting other polymers bringing additional function-alities to WBC.

Keywords Nanocellulose · Poly(*N*-isopropylacrylamide) · Polymer brushes · Swelling

Rasim Alosmanov and Karol Wolski have contributed equally to this work.

R. Alosmanov
Department of Chemistry, Baku State University,
Z. Khalilov Str. 23, AZ1148 Baku, Azerbaijan

R. Alosmanov · K. Wolski · S. Zapotoczny (✉)
Faculty of Chemistry, Jagiellonian University, Ingardena 3, 30-060 Krakow, Poland
e-mail: zapotocz@chemia.uj.edu.pl

Introduction

Cellulose is the most common, renewable, biodegradable natural polymer resource on earth. Novel demanding biomedical applications have brought more attention to this chemically well-recognized material but in a new structural form called nanocellulose. Nanocellulose is the nanostructured product or extract from the native cellulose found in plants, animals, and bacteria. Three main types of nanocellulose have been identified: cellulose nanocrystals (CNCs), nanofibrillated cellulose (NFC) and bacterial cellulose (BC) (Habibi 2014; Dufresne 2012; Klemm et al. 2011).

BC is produced by bacteria such as *Acetobacter*, *Rhizobium*, *Agrobacterium*, *Aerobacter*, *Achro-mobacter*, *Azotobacter*, *Salmonella*, *Escherichia*, and

Springer

Sarcina by cultivation in appropriate aqueous culture media (Shoda and Sugano 2005). BC has a unique and complex three-dimensional porous network structure. BC demonstrates a series of distinguished structural features and properties such as high purity, a high degree of polymerization, high crystallinity, water content up to 99%, and good mechanical stability. These properties have attracted significant interest from both research scientists and industrialists. BC has wide applications in various fields including: medical, food, advanced acoustic diaphragms, etc. (Klemm et al. 2011; Czaja et al. 2007).

Thanks to the presence of many hydroxyl groups on the BC surface its modification by various chemical treatments such as acetylation, phosphorylation, and amidation is readily available (Hu et al. 2014). Such modification of the BC surface can improve its compatibility with different matrices and expand its utilization in nanotechnology-related applications. Besides this, different guest substrates including small molecules, inorganic nanoparticles, nanowires, and polymers can be incorporated onto the surfaces of BC in order to prepare various functional nanocomposites with the desired properties or significantly improved physicochemical, catalytic, optoelectronic, and magnetic properties. Materials based on BC and its derivatives have been successfully applied in wound healing and regenerative medicine, for example (Sulaeva et al. 2015; Habibi 2014; Hu et al. 2014).

BC has been commercialized in various forms so far. Lenselink and Andriessen, for example, commercialized BC as wet bacterial cellulose (WBC) sheets. WBC sheets are characterized by desired properties such as porous structure, high water storage ability, biocompatibility and high crystallinity (Kucinska-Lipka et al. 2015). Therefore, this material has been commonly applied in skin regenerative medicine, as wound dressings, scaffolding for tissue engineering as well as the food and cosmetics industries, for example (Keshk 2014; Lenselink and Andriessen 2011). However, WBC sheets dry relatively quickly, especially at elevated temperatures, and high crystallinity reduces their reswelling ability, which significantly limits their applications as well as conditions at which they can be modified (Ul-Islam et al. 2012; Nakayama et al. 2004).

While modifications of CNC, NFC and BC have been widely reported (Sulaeva et al. 2015; Habibi 2014; Hu et al. 2014), there are only several examples

of surface modifications of WBC (Keshk 2014; Lenselink and Andriessen 2011). WBC sheets were functionalized by silanization with 3-(azidopropyl)triethoxysilane and then modified by Cu^I-catalyzed click chemistry (Hettegger et al. 2015a). In another work, two different xanthene dyes (Rose Bengal and Eosin Y) were covalently attached to premodified WBC sheets via a heterogeneous click chemistry approach (Hettegger et al. 2015b).

Polymer brushes can be obtained by two main strategies called "grafting to" and "grafting from," but only the latter leads to the formation of dense brushes (Kim et al. 2015). In the first step of this approach, a surface is functionalized with an initiator monolayer. In the second step, surface-initiated polymerizations are realized, leading to the growth of the polymer brush directly from the surface. The "grafting from" method is mostly represented by surface-initiated controlled radical polymerizations (SI-CRP) (Barbey et al. 2009), while atom transfer radical polymerization (SI-ATRP) has been the most commonly used on numerous surfaces. PNIPAM is an example of a thermosensitive polymer that may completely change its properties in response to the temperature changes (Plunkett et al. 2006). Below 32 °C in water (the value of the lower critical solution temperature, LCST), PNIPAM chains adopt extended conformation with highly hydrated chains, while above this temperature the polymer chains collapse repealing some water molecules (Benetti et al. 2007; Pelton 2010). The switchable structural changes of the PNIPAM and LCST value close to physiological temperature (which may be further tuned by copolymerization with some other monomers) are desired, especially for biomedical applications (Guan and Zhang 2011). Surface-tethered PNIPAM brushes are especially attractive materials that can be easily synthesized via the ATRP method on different surfaces, e.g., flat gold surfaces (Sui et al. 2011), aluminum oxide (Szuwarzyński et al. 2013), or polymer nanoparticles (Men et al. 2013).

In this work, we present for the first time the surface modification of WBC sheets by a thermosensitive polymer, poly(*N*-isopropylacrylamide) (PNIPAM), which was grafted to improve the swelling-drying ability of WBC. A series of swelling-drying experiments indeed indicated that the modified WBC sheets exhibited significantly improved water storage properties compared to native WBC sheets.

Experimental section

Materials

WBC sheets were kindly supplied by Biovico Co. (Gdynia, Poland) and were used as received without any pretreatment. Tetrahydrofuran (p.a.) and methanol (p.a.) were purchased from Chempur (Piekary Slaskie, Poland) and used as received. All other chemicals were purchased from Sigma-Aldrich (St. Louis, MO, USA): 3-aminopropyl-trimethoxysilane (APTES), 2-bromoisobutylyl bromide (BIB) (98%), copper (I) bromide (99.999%), bis(2-dimethylaminoethyl)(methyl)amine (PMDETA) (99%), triethylamine (TEA) (>99%), and ethanol (p.a.). N-isopropylacrylamide (97%) was purchased from Sigma-Aldrich and purified twice with recrystallization from n-hexane prior to use.

Methods

WBC sheets and the obtained derivatives were characterized by FTIR spectroscopy using a Thermo Nicolet iS10 FTIR spectrometer (Thermo Scientific) with an ATR accessory (SMART iTX). All the samples were analyzed after vacuum drying. The obtained spectra were baseline corrected and normalized using Omnic v9.0 software (Thermo Scientific). Atomic Force Microscope (AFM) images were obtained with a Dimension Icon AFM (Bruker, Santa Barbara, CA) working in the PeakForce Tapping (PFT) and QNM® mode with standard silicon cantilevers for measurements in air (nominal spring constant of 0.4 N/m). The samples were stretched and dried in air prior to imaging. Elemental analyses were performed on a Vario Micro Cube Elemental Microanalyzer (Elementar, Germany). Powder X-ray diffraction (XRD) patterns were collected on a PANalytical X'Pert PRO MPD diffractometer with Debye-Scherrer geometry using CuKα radiation ($\lambda = 1.54187$ Å; 2θ range 3°–85° for RT).

Modification of WBC sheets with APTES

The treatment of WBC sheets with silane was carried out in an ethanol solution of APTES (10 vol%) leading to the formation of WBC grafted with APTES (WBC-g-APTES). WBC sheets were place in the solutions for 24 h at room temperature. The obtained WBC-g-APTES was washed with ethanol five times by shaking (5 × 30 min) to remove possible impurities of unbound APTES.

Immobilization of initiator on WBC-g-APTES

In a typical experiment, the freshly obtained WBC-g-APTES (ca. 0.22 g) was immersed in the solvent mixture, containing 10 ml of THF and 0.4 ml of TEA. Then, BIB (0.370 ml) was added dropwise via a syringe to the reaction flask under argon atmosphere. The reaction flask was kept for an hour at room temperature. The obtained sample, WBC-g-BIB, was washed with copious amounts of THF and water.

Grafting of PNIPAM from WBC-g-BIB

PNIPAM brushes were grafted from WBC-g-BIB via the SI-ATRP method. The typical reaction system was composed of three glass vessels sealed with rubber septa and connected to each other with double-tipped needles to transfer the monomer solution under argon atmosphere. The solvent mixture of methanol/water (1:1 v/v, total volume 3 ml) containing NIPAM (1.753 g) and PMDETA (0.25 ml) was prepared in the first vial. In the second one, CuBr (23.09 mg) and a magnetic stirring bar were placed, while a WBC-g-BIB sheet was placed in the last vial. The reaction system was then purged with argon. After 30 min, the degassed mixture of the monomer and ligand from the first vial was transferred via a cannula in the flow of argon to the second vial with CuBr. The mixture was stirred at ambient temperature for 20 min to dissolve the CuBr. The obtained solution was then transferred to the last vial with WBC-g-BIB to start the ATRP process. The mixture was left to react for 24 h at ambient temperature without stirring. The resulting product, WBC-g-PNIPAM, was purified from the unbound free polymer and residual salts by washing several times with methanol and water.

Drying-swelling tests

Before drying-swelling tests, the sample (WBC-g-PNIPAM or native WBC sheet) was immersed in deionized water and shaken at room temperature. After 12 h the sample was taken out, gently removing the excess of water on the sample, and placed in an open beaker at room temperature, and its mass was followed to measure the water loss. Afterwards, the

sample was immersed again in water for 12 h at room temperature. The same procedure was repeated three times at room temperature (3 cycles). After this, the sample was dried at 40 °C up to a constant mass. Then, the sample was immersed again in water for 12 h at room temperature, and the drying-swelling procedure was repeated (3 cycles). Changes of mass at a given time, t, were used to determine the following parameters (Eqs. 1, 2):

$$M_t^i(\%) = \frac{m_D^i}{m_W^i} \times 100 \qquad (1)$$

$$M_t(\%) = \frac{m_D^i}{m_W} \times 100 \qquad (2)$$

where m_W^i and m_D^i are the initial masses of the wet sample at the beginning of each cycle (i) and the mass of the dry sample at the end of each cycle, respectively; m_W is the initial mass of the wet sample at the beginning of the drying-swelling cycle. In addition, the relative reswelling capacities of the samples after each drying-swelling cycle were calculated according to the equation:

$$C_W^{i+1}(\%) = \frac{m_W^{i+1} - m_D^i}{m_D^i} \times 100 \qquad (3)$$

Results and discussion

Formation of the PNIPAM brushes grafted via SI-ATRP from the surface of WBC sheets in the first step required immobilization of an appropriate ATRP initiator on WBC sheets. Due to the susceptibility of WBC to the reduction of its reswelling ability after substantial dehydration, the whole modification procedure and polymerization condition were adjusted to prevent such drying. The applied three-step synthetic route is shown schematically in Scheme 1.

Preparation of WBC sheets with immobilized initiators

In the first step (Scheme 1), APTES molecules containing terminal amine groups were attached via alkoxy groups to WBC hydroxyl groups. Successful attachment of APTES was confirmed by FTIR analysis (Fig. 1). The IR spectrum of WBC contains a broad band in the range of 3400–3300 cm^{-1} that is attributed to the stretching vibrations of the OH groups of cellulose that are also involved in the formation of hydrogen bonds (broadening of the band) and the band around 2900–2800 cm^{-1} corresponding to C–H stretching (Ullah et al. 2016; Amin et al. 2012). The peaks observed at 1428 and 1315 cm^{-1} are attributed to the symmetric bending of CH$_2$ and the bending vibrations of the C–H and C–O groups of the rings in polysaccharides, respectively. The bands in the range of 1000–1200 cm^{-1} are attributed to C–O stretching and C–H rocking vibrations of the pyranose ring skeleton (Alemdar and Sain 2008; Sain and Panthapulakkal 2006).

The presence of APTES in WBC-g-APTES may be deduced from the absorption band at 1566 cm^{-1}, which is the characteristic of –NH$_2$ bending vibrations. As shown in the region of 1000–1200 cm^{-1} besides the bands of the C–O stretching of cellulose, the new strong bands appeared. These strong bands were assigned to the Si–O–C$_{cellulose}$ and polysiloxane bands. Furthermore, the intensity of the IR band assigned to cellulose O–H stretching vibrations (about 3342 cm^{-1}) was slightly reduced, indicating covalent attachment of APTES molecules to the WBC surface. A weak band at 2940 cm^{-1} may be assigned to the CH$_2$ groups of APTES (Matias et al. 2000).

WBC-g-APTES was reacted with BIB in THF in the presence of TEA (Scheme 1, step 2), leading to the formation of initiator-decorated WBC-g-BIB. The successful modification was also confirmed by FTIR (Fig. 1). Comparing the FTIR spectra of WBC-g-APTES and WBC-g-BIB, one may notice the biggest changes especially in the range of 1000–1800 cm^{-1}. In the mentioned region, the presence of new peaks at 1654 and 1530 cm^{-1} was observed and assigned to the formation of the amide groups between APTES and BIB.

Grafting of PNIPAM brushes from the WBC-g-BIB sheet

The obtained WBC-g-BIB sheet was then used for SI-ATRP of NIPAM (Scheme 1, step 3). The grafting of PNIPAM was followed by FTIR, AFM, and elemental analysis methods. Successful formation of PNIPAM brushes on the WBC sheet was evidenced by the appearance of new peaks at 1642 and 1538 cm^{-1}, corresponding to the amide I and amide II stretch

Scheme 1 Schematic presentation of the formation of PNIPAM brushes on WBC sheets: APTES grafting (first step), BIB treatment (second step) and SI-ATRP of NIPAM (last step)
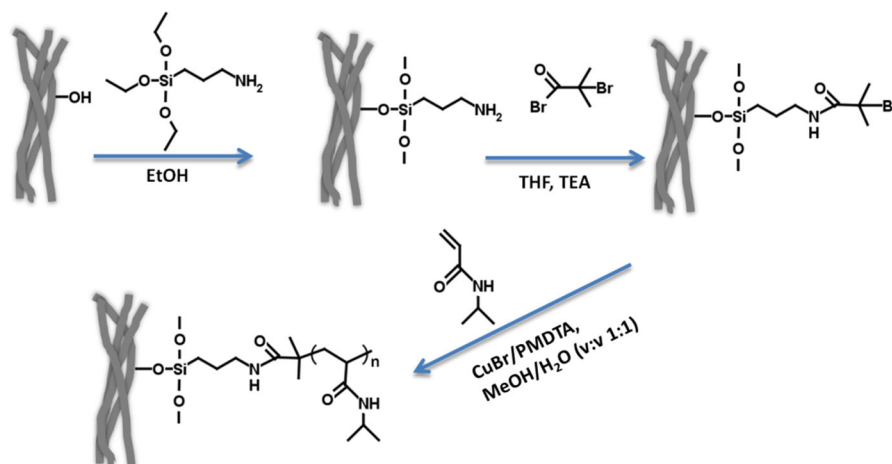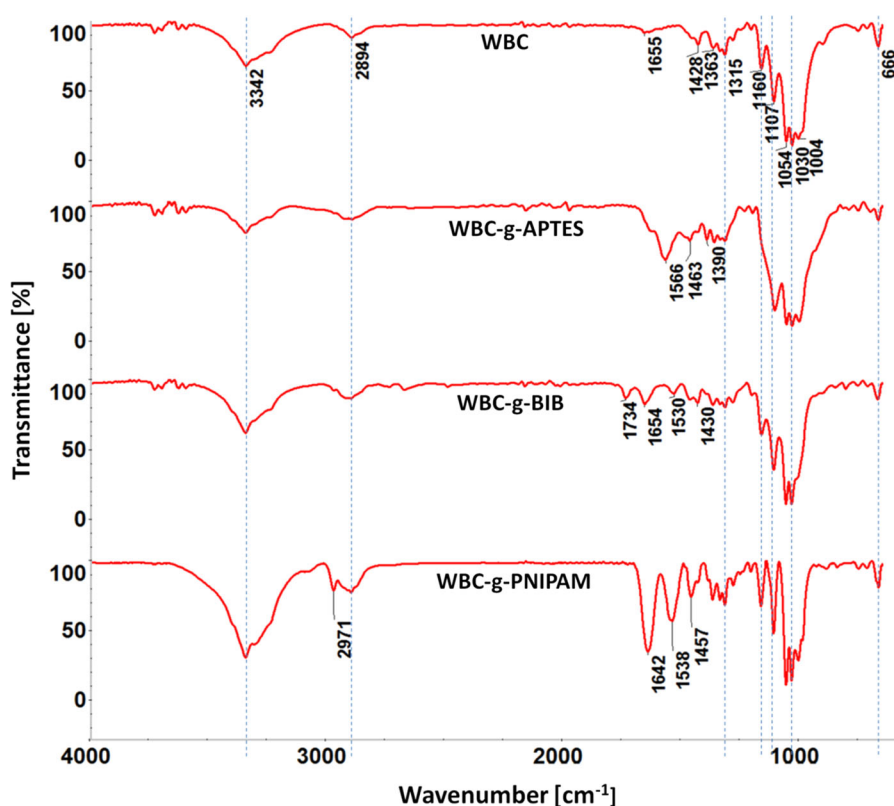

Fig. 1 Normalized FTIR spectra of the initial WBC sheet and after further modifications with APTES (WBC-g-APTES) and BIB (WBC-g-BIB) and SI-ATRP of NIPAM (WBC-g-PNIPAM)

vibrations in PNIPAM as well as the peak at 2971 cm^{-1} corresponding to the C–H stretch of the isopropyl group. Moreover, the intensity of the band with the maximum at about 3340 cm^{-1} was significantly increased because of the presence of amide groups in PNIPAM chains (the bands assigned to N–H stretching vibrations overlap with the bands that come from O–H stretching vibrations). Substantial broadening of the mentioned band may be assigned to the

formation of hydrogen bonds between the PNIPAM chains and BC surface. The AFM image of the native WBC sheet (see Fig. 2A) clearly shows the fibrilar structure of the material. After the formation of PNIPAM brushes on the WBC sheet, the topography of the sample was completely changed (see Fig. 2B). The formed PNIPAM layer can be easily recognized; however, the brush layer does not seem to be uniform. The possible explanation of this phenomenon is related

Fig. 2 AFM topography images in air of **A** the native WBC sheet and **B** WBC-g-PNIPAM
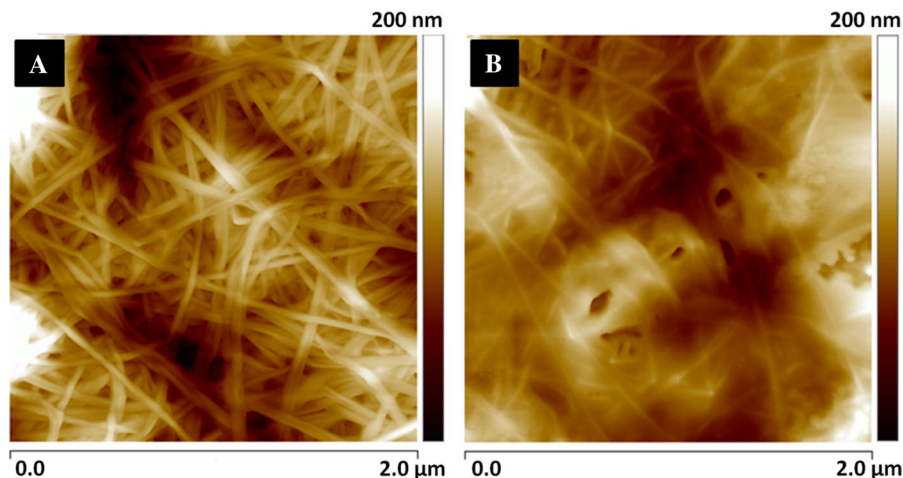
to changes of the sample shape during the drying process. Macroscopically, the WBC sheets are flat and rather smooth, while dried samples are strongly mangled. Moreover, sample preparation for AFM measurements requires stretching of the sample before its fixation to a solid substrate. The elemental analysis of the initial WBC (C- 43.7%, H- 6.42% and N- 0.22%) and WBC-g-PNIPAM (C- 46.8%, H- 6.98% and N-2.2%) revealed that WBC-g-PNIPAM contains about 22% of PNIPAM with respect to the dry sample.

The crystalline structures of the nanocellulose samples were studied using powder X-ray diffraction (XRD). The diffractograms of WBC and WBC-g-PNIPAM were found to be virtually identical (see Fig. 3), both showing only two diffraction peaks with maxima at ca. 14.4° and 22.6°. The results showed that grafting of PNIPAM brushes from WBC sheets did not reduce the original crystallinity of the nanocellulose fibers, and no additional phase was formed. Such observations indicated that the applied chemical modifications involved essentially hydroxyl groups on the fibers' surface or those in the amorphous regions of WBC, while the internal structure of the fibers was not affected (Tomé et al. 2011; Lee et al. 2011). A similar phenomenon was reported for surface modification of nanocellulose by organic acids (Ramírez et al. 2014) and trimethylchlorosilane (Sai et al. 2015), for example.

Drying-swelling tests

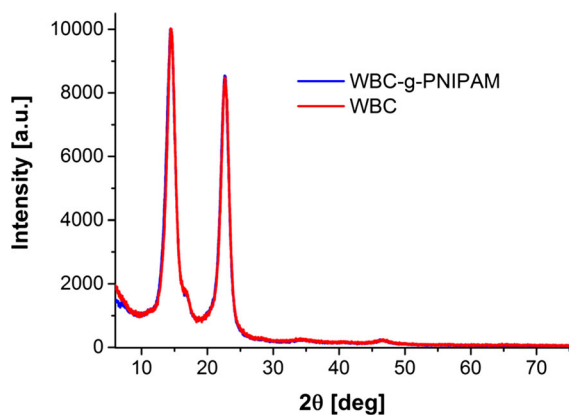Drying-swelling tests were carried out to study the reswelling ability of the WBC and WBC-g-PNIPAM

Fig. 3 XRD diffractograms of WBC and WBC-g-PNIPAM sheets

sheets. The results of the experiments can be presented using two approaches. In the first case, the mass loss was calculated taking into account the starting conditions for each drying-swelling cycle using Eq. 1 (see Fig. 4A, B), while in the second approach all the calculations referred to the starting masses (see Fig. 4C, D). As can be seen in Fig. 4A (cycles 1–3), drying proceeded much more slowly for WBC-g-PNIPAM than for WBC sheets. The grafted PNIPAM seems to protect WBC sheets from drying so after ca. 500 min native WBC loses ca. 20% more water than WBC-g-PNIPAM. Water molecules located inside the sample were prevented from the fast evaporation because of the presence of the protective PNIPAM layer (see Scheme 2). Importantly, this behavior was not limited to a single drying cycle, but was preserved. These results could be attributed to the fact that the
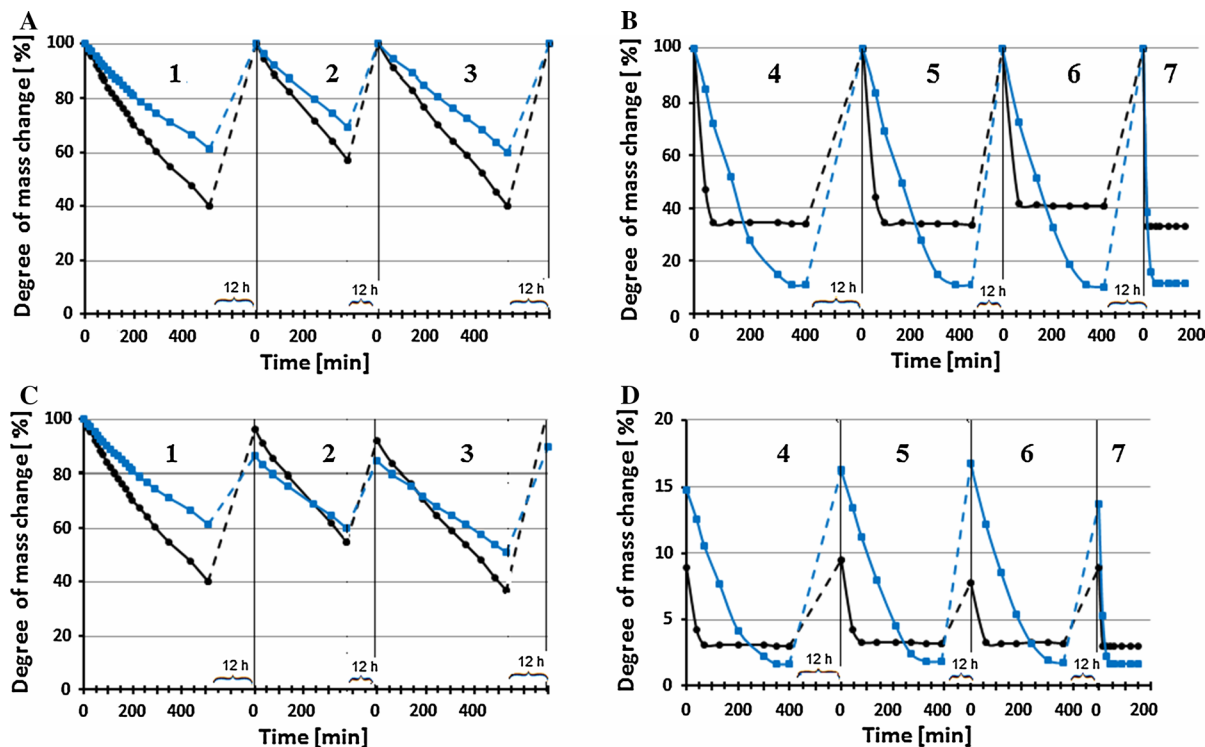
Fig. 4 Degree of mass change (%) measured in time during several drying-swelling tests performed at room temperature (*black lines* WBC sheets, *blue lines* WBC-g-PNIPAM sheets, *continuous lines* drying steps, *dotted lines* wetting steps). **A,**

B Calculated based on Eq. (1); **C, D** calculated based on Eq. (2). Between the 3rd and 4th cycles, the samples were dried for 1 h at 40 °C. (Color figure online)

layer of thermosensitive PNIPAM chains is well hydrated at room temperature and is less prone to losing water molecules than crystalline WBC. Importantly, as reported above, no changes in the degree of crystallinity could be noticed after grafting of PNIPAM brushes. It means that the contribution of the crystallinity of the fibers to the swelling/drying ability was also the same for both samples, and the reported differences may only be assigned to the presence of PNIPAM brushes.
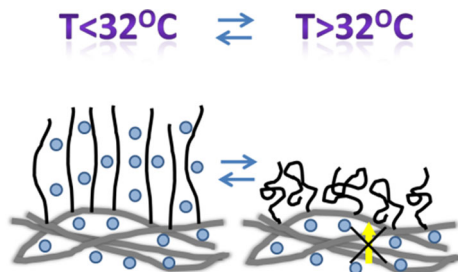
Scheme 2 Schematic drawing of the protective PNIPAM shell on WBC below and above PNIPAM LCST

However, the water storage capacity of WBC-g-PNIPAM is slightly lower than that of native WBC. The WBC-g-PNIPAM sheet after the first drying-swelling cycle reaches ca. 85% of its original mass, while WBC swells more, reaching 90–95% of its original mass (see Fig. 4C). It seems that the PNIPAM layer slightly limits the total hydration level of the material, but a positive effect on the drying rate at room temperature is crucial and more pronounced.

After three drying-swelling cycles at room temperature, the samples were left to dry at 40 °C for 1 h and reswollen, and subsequently the same three cycles were followed at room temperature. Drying at 40 °C significantly reduced the masses of WBC (to 9% of the original mass) and WBC-g-PNIPAM (to 15%) and influenced the subsequent drying profile (cycles 4–7 in Fig. 4B, D). It appears that WBC-g-PNIPAM is able to hold more water than WBC even after prolonged drying at elevated temperature (close to the physiological one). More importantly, the drying profiles indicated that WBC lost its water storage ability and

was only able to keep water molecules adsorbed on the surface (they evaporate very quickly). In contrast, the swelling properties of WBC-g-PNIPAM were only slightly affected—the sample reached constant mass upon drying, lasting more than 400 min, and was still able to reswell. It is clear that PNIPAM brushes exhibit a protective effect for WBC sheets during drying at 40 °C. At this temperature (above LCST), PNIPAM chains adopt a collapsed conformation, and the surface becomes less hydrated, which may prevent water molecules from being transported from the bulk WBC to the surface and evaporated (Scheme 2). The final monitored drying cycle at 40 °C showed that even though the drying of both samples at this elevated temperature proceeds quickly, the PNIPAM layer seems to protect WBC from irreversible drying as shown in the 4–6 cycles succeeding this drying step. The effect is more pronounced if one compares the reswelling capacities of the samples, as calculated using Eq. (3) (Fig. 5). Apparently, after drying at room temperature, the reswelling capacity of WBC-g-PNIPAM is smaller than that of WBC. This can be partially rationalized by the fact that WBC loses more water than WBC-g-PNIPAM during drying, so to restore its weight, it also absorbs relatively more water. However, the advantage of the protective effect of PNIPAM can be clearly seen after drying the samples at elevated temperature. For drying-swelling cycles 4–6, the relative reswelling capacity of WBC-g-
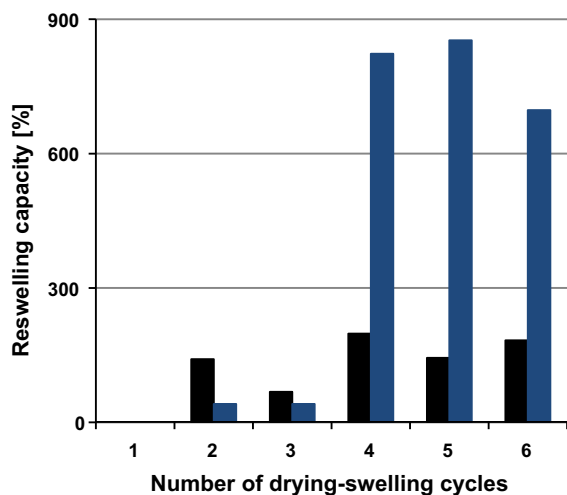
PNIPAM was found to be even ca. four times larger than the one observed for native WBC.

Conclusion

In the present work, poly(*N*-isopropylacrylamide) brushes were successfully grafted from wet bacterial cellulose sheets via ATRP. The applied method resulted in the formation of the PNIPAM layer on the surface of WBC, which protected it from fast drying and enabled its reswelling even after drying at elevated temperature, which commonly leads to irreversible drying of native WBC. All the modification steps were confirmed using FTIR, elemental analysis and AFM imaging. The reported observations may be explained by the thermoresponsive behavior of PNIPAM chains, which at room temperature are well hydrated, enabling the swelling of WBC but also slowing down its drying. What is more, above 32 °C (LCST value) PNIPAM chains become less hydrated, forming a barrier for water molecules trying to escape from WBC. The reported modification of WBC significantly broadens the range of applications of this biocompatible, natural material, slowing down its drying at relevant temperatures close to the physiological one. It also paves the way for grafting other brushes from the surface of WBC that can bring new functionalities to nanocellulose.

Fig. 5 The relative reswelling capacity of the samples as determined using Eq. (3) for the consecutive drying-swelling cycles described in Fig. 4 (WBC *black bars*; WBC-g-PNIPAM *blue bars*). (Color figure online)

References

Alemdar A, Sain M (2008) Isolation and characterization of nanofibers from agricultural residues: wheat straw and soy hulls. Bioresour Technol 99:1664–1671

Amin I, Ahmad N, Halib N, Ahmad I (2012) Synthesis and characterization of thermo- and pH-responsive bacterial cellulose/acrylic acid hydrogels for drug delivery. Carbohydr Polym 88:465–473

Barbey R, Lavanant L, Paripovic D, Schuwer N, Sugnaux C, Tugulu S, Klok HA (2009) Polymer brushes via surface-initiated controlled radical polymerization: synthesis, characterization, properties, and applications. Chem Rev 109:5437–5527

Benetti EM, Zapotoczny S, Vancso GJ (2007) Tunable thermoresponsive polymeric platforms on gold by "photoiniferter"-based surface grafting. Adv Mater 19:268–271

Czaja WK, Young DJ, Kawecki M, Brown RM (2007) The future prospects of microbial cellulose in biomedical applications. Biomacromolecules 8:1–12

Dufresne A (2012) Nanocellulose. From nature to high performance tailored materials. Walter de Gruyter GmbH, Berlin/Boston, p 460

Guan Y, Zhang Y (2011) PNIPAM microgels for biomedical applications: from dispersed particles to 3D assemblies. Soft Matter 7:6375–6384

Habibi Y (2014) Key advances in the chemical modification of nanocelluloses. Chem Soc Rev 43:1519–1542

Hettegger H, Sumerskii I, Sortino S, Potthast A, Rosenau T (2015a) Silane meets click chemistry: towards the functionalization of wet bacterial cellulose sheets. Chem Sus Chem 8:680–688

Hettegger H, Gorfer M, Sortino S, Fraix A, Bandian D, Rohrer C, Harreither W, Potthast A, Rosenau T (2015b) Synthesis, characterization and photo-bactericidal activity of silanized xanthene-modified bacterial cellulose membranes. Cellulose 22:3291–3304

Hu W, Chen S, Yang J, Li Z, Wang H (2014) Functionalized bacterial cellulose derivatives and nanocomposites. Carbohydr Polym 101:1043–1060

Keshk S (2014) Bacterial cellulose production and its industrial applications. J Bioprocess Biotech 4:150–160

Kim M, Schmitt SK, Choi JW, Krutty JD, Gopalan P (2015) From self-assembled monolayers to coatings: advances in the synthesis and nanobio applications of polymer brushes. Polymers 7:1346–1378

Klemm DF, Kramer F, Moritz S, Lindstrom T, Ankerfors M, Gray D, Dorris A (2011) Nanocelluloses: a new family of nature-based materials. Angew Chem Int Ed 50:5438–5466

Kucinska-Lipka J, Gubanska I, Janik H (2015) Bacterial cellulose in the field of wound healing and regenerative medicine of skin: recent trends and future prospective. Polym Bull 72:2399–2419

Lee KY, Quero F, Blaker JJ, Hill CAS, Eichhorn SJ, Bismarck A (2011) Surface only modification of bacterial cellulose nanofibers with organic acids. Cellulose 18:595–605

Lenselink E, Andriessen A (2011) A cohort study on the efficacy of a polyhexanide-containing biocellulose dressing in the treatment of biofilms in wounds. J Wound Care 20:536–539

Matias MC, De La Orden MU, Sannchez CG, Urreaga JM (2000) Comparative spectroscopic study of the modification of cellulosic materials with different coupling agents. J Appl Polym Sci 75:256–266

Men Y, Drechsler M, Yuan J (2013) Double-stimuli-responsive spherical polymer brushes with a poly(ionic liquid) core and a thermoresponsive shell. Macromol Rapid Commun 34:1721–1727

Nakayama A, Kakugo A, Gong JP, Osada Y, Takai M, Erata T, Kawano Sh (2004) High mechanical strength double-network hydrogel with bacterial cellulose. Adv Funct Mater 14:1124–1128

Pelton R (2010) Poly(N-isopropylacrylamide) (PNIPAM) is never hydrophobic. J Colloid Interface Sci 348:673–674

Plunkett KN, Zhu X, Moore JS, Leckband DE (2006) PNIPAM chain collapse depends on the molecular weight and grafting density. Langmuir 22:4259–4266

Ramírez JAA, Suriano CJ, Cerrutti P, Foresti ML (2014) Surface esterification of cellulose nanofibers by a simple organocatalytic methodology. Carbohydr Polym 114:416–423

Sai H, Fu R, Xing L, Xiang J, Li Z, Li F, Zhang T (2015) Surface modification of bacterial cellulose aerogels' web-like skeleton for oil/water separation. ACS Appl Mater Interfaces 7:7373–7381

Sain M, Panthapulakkal S (2006) Bioprocess preparation of wheat straw fibers and their characterization. Ind Crop Prod 2:1–8

Shoda M, Sugano Y (2005) Recent advances in bacterial cellulose production. Biotechnol Bioprocess Eng 10:1–8

Sui X, Zapotoczny S, Benetti EM, Memesa M, Hempeniusa MA, Vancso GJ (2011) Grafting mixed responsive brushes of poly(N-isopropylacrylamide) and poly(metacrylic acid) from gold by selective initiation. Polym Chem 2:879–884

Sulaeva I, Henniges U, Rosenau T, Potthast A (2015) Bacterial cellulose as a material for wound treatment: properties and modifications. A review. Biotechnol Adv 33:1547–1571

Szuwarzyński M, Zaraska L, Sulka GD, Zapotoczny S (2013) Pulsalite releasing platform of nanocontainers equipped with thermally responsive polymeric nanovalves. Chem Mater 25:514–520

Tomé LC, Freire MG, Rebelo LPN, Silvestre AJD, Neto CP, Marrucho IM (2011) Surface hydrophobization of bacterial and vegetable cellulose fibers using ionic liquids as solvent media and catalysts. Green Chem 13:2464–2470

Ul-Islam M, Khan T, Park JK (2012) Water holding and release properties of bacterial cellulose obtained by in situ and ex situ modification. Carbohydr Polym 88:596–603

Ullah MW, Ul-Islam M, Khan S, Kim Y, Park JK (2016) Structural and physico-mechanical characterization of biocellulose produced by a cell-free system. Carbohydr Polym 136:908–916